Filter design for folded canonical topologies based on equivalent circuit segmentation

Antonio Romera Perez[a], Alejandro Pons Abenza[a], David Martinez Martinez[b], Alejandro Alvarez Melcon[a], Fernando D. Quesada Pereira[a,*]

[a]*Communications and Information Technologies Department, Universidad Politécnica de Cartagena, Campus de la Muralla del Mar s/n, Cuartel de Antigones, Cartagena 30202, Spain. emails: antoniorp89@gmail.com; alejandroponsabenza@gmail.com; alejandro.alvarez@upct.es; fernando.quesada@upct.es*

[b]*Inria Sophia Antipolis-Méditerranée, 2004 route des Lucioles-BP 93 06902, France. email: david.martinez@inria.fr*

Abstract

This paper presents a methodology to design filters with folded canonical topologies, which implement cross couplings between non-adjacent resonators. The technique is based on segmenting the traditional coupling matrix in a step-by-step fashion. At each step, a subset of the whole physical structure is optimized to match the response of the corresponding segment of the coupling matrix. In the context of this design technique, in this paper we propose an efficient segmentation methodology of the coupling matrix based on multiport networks. The use of multiport networks allows to generate at each step several goal functions, which are simultaneously used during the optimization of the corresponding physical segment. These multiport networks allow to efficiently monitor the different paths of the signal, present in folded canonical topologies. It is shown that this strategy leads to a fast convergence of the step-by-step segmentation technique for the design of this type of coupling topologies. We apply the proposed methodology to the design of two filters using the quartet topology. The first filter has two transmission zeros placed at the real frequency axis, and the second one has two complex transmission zeros intended for group delay equalization. The results indicate that the proposed methodology is effective for the design of this type of coupling topologies, leading to initial dimensions for the filters that typically have less than 1% of error when they are compared with those obtained from a final global optimization.

*fernando.quesada@upct.es

Manuscript accepted in International journal of electronics and communications 2019

Keywords: Bandpass filters, Coupling Matrix, Optimization techniques, Design techniques, Rectangular waveguide filters

1. Introduction

The design of microwave filters has traditionally been considered to be a very time consuming activity, mainly because full wave complex computational software is usually needed in order to perform a large number of simulations. These simulations have high computational costs, and therefore it is necessary to use efficient design techniques to minimize the time that is needed for the full production of this type of hardware. Although some techniques are available to obtain initial dimensions of filters [1, 2], they usually require a final optimization of the whole structure, until the required response is finally obtained. However, for complex filter topologies, optimization techniques may find difficulties in convergence, specially if the initial designs are far from the desired target specifications.

The classical technique presented in [3] models coupling elements and cavities separately. However, after assembling the filter, undesired interactions between resonators and coupling elements are usually present. Therefore, final global optimizations are required. The success of these optimization processes will mainly depend on the quality of the achieved initial design. This is specially true for optimization techniques based on gradient algorithms, which traditionally need initial dimensions of the filter very close to the optimum solution. Otherwise, they are easilly trapped into local minima, thus making the convergence to optimum solutions very problematic.

Another possibility is to use Genetic Algorithms (GA) for microwave filters design [4, 5, 6, 7]. They are based on selection mechanisms, which avoid the problem of local minima that is inherent to gradient algorithms. However, the high number of iterations required by these algorithms leads to a significant computational cost. Space mapping optimization techniques are also useful options for efficient filter design tasks [8, 9, 10, 11]. This kind of techniques connects two models, coarse and fine, and sometimes it is difficult to find a good mapping between them. This is especially true if a strong mis-alignment is present between the fine and coarse models. These techniques, therefore, rely in how good the coarse models are with respect to the corresponding fine models.

There are some alternative design techniques that are based on deriving equivalent circuits of the filter. For instance, in [12] a waveguide iris width is computed to match the response of a circuit prototype in magnitude and phase. Even though it shows good convergence, it does not consider any of the couplings and interactions from nearby elements. Thus, after assembling all parts of the filter, the response usually presents significant deviations with respect to the target response. Also, authors in [13] use an equivalent circuit to design a dual-mode circular waveguide filter in quartet topology, with one cross coupling. The technique first adjusts individually the coupling irises and the resonators of the structure along the main path. As a final step, it proposes the adjustment of the iris along the cross coupling path with the help of an equivalent circuit. The technique results to be very accurate, since the final adjustment of the cross coupling is done with an equivalent circuit that takes into account the influence of nearby elements. However, it would be difficult to extend the proposed technique to higher order networks, or to topologies that include additional cross couplings.

A step by step procedure, presented in [14, 15], shows a different technique to design waveguide filters. This procedure consists in obtaining an equivalent circuit that represents the complete microwave filter with the desired specifications. At each step, the circuit is segmented as needed. For inline filters, the process begins dimensioning the input coupling and first resonator, and continues adding coupling structures and resonators one by one. At each step, the physical sub-structure is optimized to match the response of the corresponding segment of the equivalent circuit. A reduced number of elements is optimized at each step (only two elements, namely the last coupling and resonator added to the structure). This technique has also been used, more recently, for the design of waveguide dual-mode filters in all inductive technology [16]. This is a complex topology that introduces cross-couplings between the two resonators hosted by one cavity with two other resonators placed in adjacent cavities.

In this paper, a similar strategy is employed for the design of complex filters using folded canonical coupling topologies. The main characteristic of these topologies is that they employ cross-couplings between non-adjacent resonators to implement transmission zeros in the filter response. Due to the introduction of these cross-couplings, the segmentation technique presented in [14, 15, 16] cannot be directly applied to this type of structures.

In this context, this paper extends for the first time the application of the segmentation technique proposed in [14, 15] to the design of microwave filters with folded canonical topologies. For this purpose, a new and efficient segmentation strategy for the equivalent circuit, including the cross-couplings that are present in the topology, is proposed. The segmentation strategy is based on considering the cross-coupling paths at different stages during the design process. Multiport goal functions are for the first time proposed in connection to the segmentation design technique. The multiport goal functions are needed to monitor the signal along the main path, and along the cross-coupling paths, simultaneously. We want to emphasize here that a proper segmentation strategy is crucial to obtain an accurate initial design of the filter, in order to minimize subsequent optimization operations. This is because it is very important to take into account the influence of key elements of the structure, during the optimization of new nearby elements.

First, the theory for scaling the coupling matrix from the normalized coupling matrix using the physical parameters of a particular filter implementation, will be reviewed. Since the theory for scaling the coupling matrix was presented before in [16], only a brief review will be presented in this work, together with final expressions needed for its practical implementation. Although in [16] the work was developed using series resonators, the final expressions in this paper will be particularized for the case of parallel resonators, which are more appropiate to represent folded canonical topologies. The novel strategy proposed for the segmentation of the equivalent circuit will then be illustrated with the design of a quartet topology. This includes how to employ multiport goal functions to take into account for cross couplings, to optimize the physical dimensions of the different segments. Contrary to [13], the extension of the proposed strategy to the design of higher order folded canonical topologies, including those with additional cross couplings, is straightforward. The derived technique has been used for the first time for the design of two filters using the quartet topology. The first quartet filter exhibits transmission zeros in the real frequency axis, while the second is designed for complex transmission zeros, intended for group delay equalization. Results for both filters show that the new segmentation strategy is very efficient, and can be used for the fast design of this type of complex filter topologies. In fact, it is demonstrated in this paper that the initial designs obtained with the proposed technique are very close to fulfill with the desired target specifications.

2. Theory

The first step to apply the proposed technique is to find an equivalent circuit of the filter to be designed. Next, the equivalent circuit will be segmented in several sub-circuits. The segments of the equivalent circuit have electrical responses which must be similar to corresponding segments of the physical structure. Therefore, the responses obtained from the sub-circuits are used as goal functions to optimize the corresponding segments of the physical structure. The segments are added one by one sequentially, until the dimensions of the whole structure are found. This will produce initial dimensions for the filter, with a response as close as possible to the desired target specifications. If refinement is needed, a final global optimization can be applied to the whole structure. This final optimization process can use, in general, efficient gradient algorithms, provided that the starting point performs closely enough to the target specifications.

To find the equivalent circuit of the filter, a scaled coupling matrix is used. This scaled coupling matrix is obtained from the normalized coupling matrix [3], using electrical parameters relevant to the technology that is going to be employed during the filter implementation. In this work, waveguide technology is used for the physical implementation, so the theory will be illustrated as applied to rectangular waveguide resonators of cross section (a, b).

The theory for the scaled coupling matrix was presented in [16]. However, in [16] equivalent circuits based on series resonator and impedance inverter were used. On the contrary, in this work, we use a dual equivalent circuit based on parallel resonators and admittance inverters. We found that for folded canonical topologies, containing cross-coupling paths, the representation with this dual version of the equivalent circuit is more convenient. This is because it leads to more straightforward representations of the equivalent circuit when the segments contain several coupling paths to account for cross-couplings. In this section, the most relevant equations will be reviewed, for this dual version of the equivalent network.

The coupling matrix is a circuit representation of a normalized lowpass prototype network, as shown in Fig. 1(a). This figure shows a circuit composed of parallel capacitors, whose values are normalized to 1 F, and also contains constant susceptances of values $(j\,B_m)$. Couplings between the elements of the network are characterized with admittance inverters of values (M_{mn}). As shown, the input/output admittance terminations are also normalized to 1 Ω^{-1}. The coupling matrix represents this normalized network, containing the constant susceptance values in the diagonal elements of the matrix $(M_{mm} = B_m)$, and the admittance inverters (M_{mn}) in the off-diagonal positions of the matrix [3]. From this normalized prototype, a scaled version

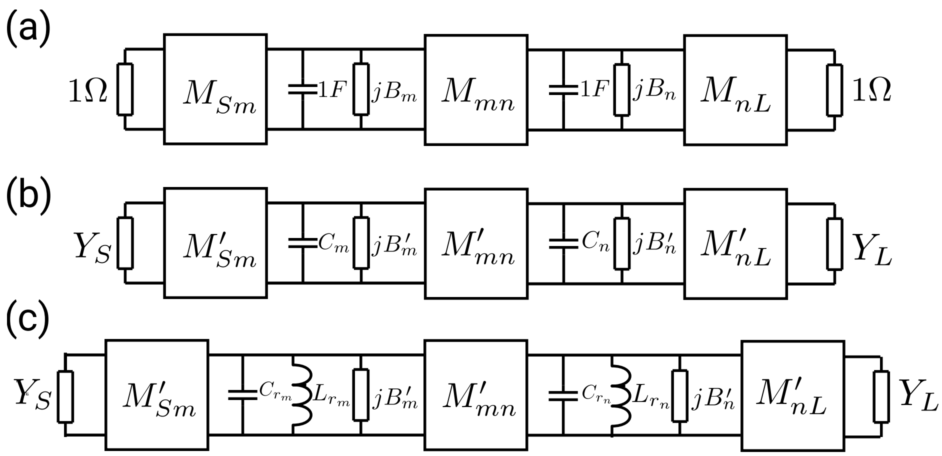

Figure 1: (a) Equivalent circuit of a normalized lowpass prototype network composed of parallel capacitors and constant susceptances, coupled by admittance inverters. (b) Lowpass filter with arbitrary input/output admittances, and scaled capacitors and constant susceptances. Admittance inverters are conveniently scaled to keep the same response as the original network. (c) Equivalent circuit of a bandpass filter obtained from (b) after applying a standard lowpass to bandpass transformation.

of the equivalent circuit can be obtained, as shown in Fig. 1(b). The input/output admittance terminations now have arbitrary values (Y_S, Y_L). In the same way, constant susceptances $(j\,B'_m)$ and capacitors are scaled with arbitrary constants (C_m). It is well known that the response of this network does not change if the admittance inverters are also scaled to convenient values (M'_{mn}) [1]. Finally, applying a standard lowpass to bandpass transformation, each capacitor is transformed into a parallel resonator $(C_{r_m},\ L_{r_m})$, as shown in Fig. 1(c). This last network represents the equivalent circuit of the bandpass filter that is going to be designed.

The key step in the described process, is to find a suitable scaling factor (C_m) to correctly represent the particular resonator that will be used in the physical implementation of the filter. To do this, we use the equivalence shown in Fig. 2. Fig. 2(a) shows a half wavelength $(\lambda_g/2)$ open-ended transmission line resonator. In our case, this transmission line represents the resonant mode (TE_{101}) in the rectangular waveguide resonator to be used in the physical implementation of the filter. The physical resonator represented in this form will be made equivalent to the parallel lumped resonator shown in Fig. 2(b). For both circuits to be equivalent, two conditions must be imposed. First, the resonant frequencies of both resonators must be the

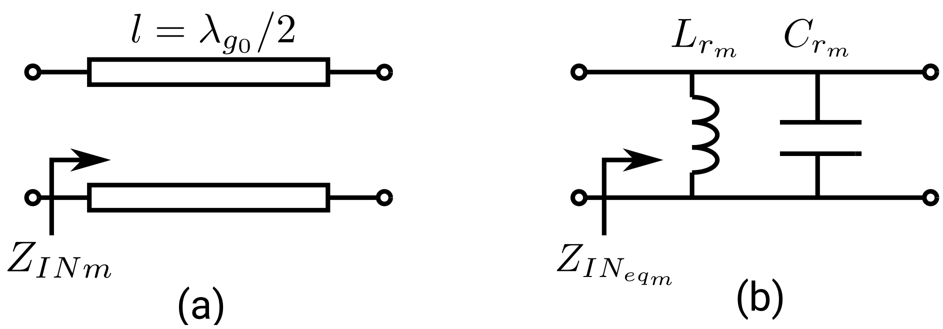

Figure 2: (a) Open ended transmission line resonator of $\lambda_g/2$ length, representing the physical rectangular waveguide resonator (resonant mode TE_{101}). (b) Lumped elements parallel resonator employed in the equivalent circuit.

same, and second the slope parameters of both resonators must be the same. With the imposition of these two conditions, the value of the inductor and capacitor for the lumped elements resonator can be computed as

$$C_{r_m} = \frac{\beta_1}{\omega_0\,\omega_{c_1}\,\mu_0}\tan(\beta_1\,l)\left(\frac{\omega_{c_1}}{\omega_0} - \frac{\omega_0}{\omega_{c_1}}\right)^{-1}, \qquad L_{r_m} = \frac{1}{\omega_0^2\,C_{r_m}}, \tag{1}$$

being (β_1) the propagation constant of the mode (TE_{10}) in the rectangular waveguide evaluated at the lower (ω_{c_1}) cut-off frequency of the passband, (l) the physical length of the resonator, and (ω_0) the center angular frequency of the filter. Note that since the resonators of the filter are implemented using the (TE_{101}) resonant mode, we will adjust the length to be

$$l = \frac{\lambda_{g_0}}{2} = \frac{\pi}{\beta_0}, \tag{2}$$

where (β_0) is the propagation constant of the mode (TE_{10}), but evaluated at the center frequency of the passband

$$\beta_0 = \sqrt{\omega_0^2\,\varepsilon_0\,\mu_0 - \left(\frac{\pi}{a}\right)^2}, \quad \beta_1 = \sqrt{\omega_{c_1}^2\,\varepsilon_0\,\mu_0 - \left(\frac{\pi}{a}\right)^2}. \tag{3}$$

Here we want to remark that for asynchronously tuned topologies, having resonators tuned to different resonant frequencies, a similar process is applied, but replacing the center frequency of the passband (ω_0) by the actual resonant frequency of each resonator (ω_{r_m}).

Having computed the elements of the resonators, the values of the capacitors (C_m) in the lowpass prototype of Fig. 1(b) are computed using, in the inverse direction, the same lowpass to bandpass transformation, obtaining

$$C_m = F_B \, \omega_0 \, C_{r_m}, \qquad F_B = \frac{\omega_{c_2} - \omega_{c_1}}{\omega_0}, \tag{4}$$

where (F_B) is defined as the fractional bandwidth of the bandpass response, and (ω_{c_2}) is the upper cutoff angular frequency of the filter. These calculated lowpass capacitors actually represent the scaling factors needed to compute the scaled coupling matrix (M'), representing the networks of Fig. 1(b) and Fig. 1(c). The elements of the scaled coupling matrix are finally calculated as

$$M'^2_{Sm} = Y_S \, C_m \, M^2_{Sm} \tag{5a}$$
$$M'^2_{mn} = C_m \, C_n \, M^2_{mn} \tag{5b}$$
$$M'^2_{nL} = C_n \, Y_L \, M^2_{nL}. \tag{5c}$$

In these expressions, (M'_{Sm}) represents the couplings from the input port to internal resonators, while (M'_{nL}) represents couplings from the output port to internal resonators. All other inter-resonators couplings are determined by (M'_{mn}). A particular case occurs when ($m = n$). In this case, the element lies in the diagonal of the coupling matrix, and it gives the scaling factor of the constant susceptances ($M'_{mm} = B'_m$). This situation is covered with the same equation (5b), shown above, which is still valid under the condition ($m = n$).

3. Design example

In this section, a fourth order filter with a quartet topology is going to be designed to illustrate the design technique. This is a folded canonical topology, which is synchronously tuned and has only one cross coupling for symmetrical responses. The topology allows the implementation of two transmission zeros in the insertion loss response of the filter. The coupling topology is shown in Fig. 3(a), while a possible physical implementation using folded rectangular waveguide technology is shown in Fig. 3(b). In Fig. 3(a) input/output ports are indicated with dashed circles, while resonators are shown with white circles marked as (R_m, $m = 1, 2, 3, 4$). The sketch also shows the couplings along the main path with solid lines, and the cross

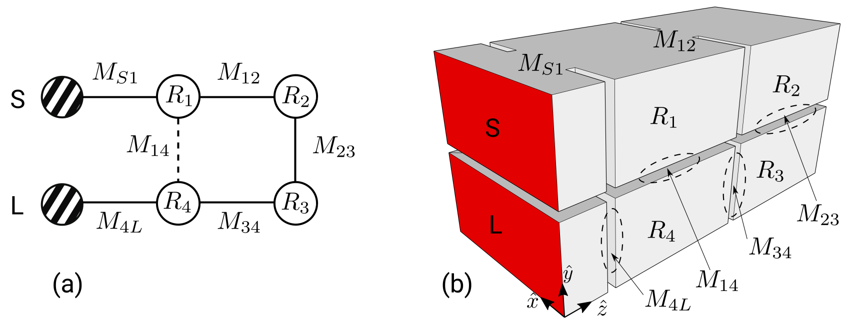

Figure 3: (a) Coupling topology of the folded canonical network selected for design. (b) Physical implementation of the filter using rectangular waveguide technology. Input (S) and output (L) ports are marked in red.

coupling with a dashed line. The correspondence between couplings with window irises, and resonators with cavities in the physical implementation, is indicated in the 3D view of Fig. 3(b). It can be observed that the physical topology is folded in the E-plane. Consequently, the couplings (M_{23}) and (M_{14}) are implemented through irises, which are open on the top and bottom walls of the corresponding waveguides. The other couplings (M_{S1}, M_{12}, M_{34}, M_{4L}) are implemented with regular inductive irises.

The basic geometry of all the irises can be further explored in the top and side views of the structure presented in Fig. 4. In these drawings, the coupling (M_{23}) is controlled with the iris width (a_3), while the coupling (M_{14}) is controlled with the iris width (a_4). The figure also shows all the geometrical parameters that will be optimized during the design process. For practical reasons, the thickness of all walls (l_i) is set to 1 mm. It is important to remark that the folding of the structure along the E-plane allows to adjust the sign of the vertical couplings. This fact makes possible the implementation of the two transmission zeros of the topology, either in the real frequency axis or in the complex plane.

For the physical implementation, we use a standard rectangular waveguide WR-75 ($a = 19.05$ mm and $b = 9.525$ mm). The filter specifications are: center frequency $f_0 = 11$ GHz, bandwidth $BW = 300$ MHz and minimum return loss $RL = 15$ dB. Also, the quartet topology has associated two transmissions zeros, that will be placed at $f_{z_1} = 10.78$ GHz and $f_{z_2} = 11.12$ GHz. As it can be noticed, the two transmission zeros are symmetrically disposed with respect to the center frequency of the filter.

The design process starts by obtaining the normalized coupling matrix

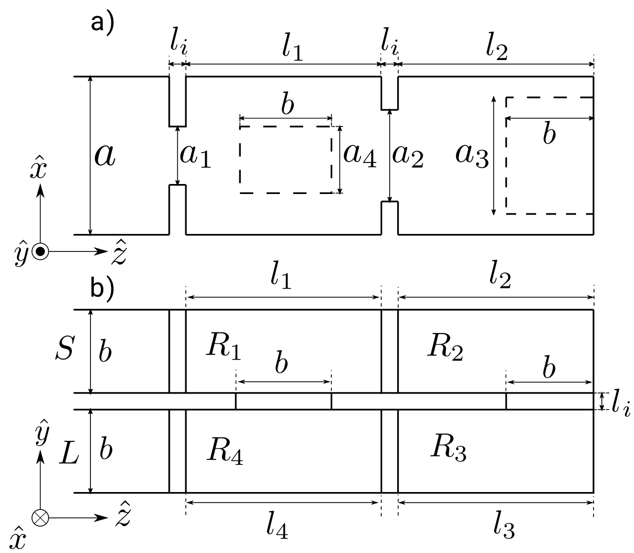

Figure 4: a) Top view of the waveguide filter, showing the relevant geometrical parameters involved in the design process. b) Side view of the waveguide filter. Due to practical considerations, the thickness of all waveguide walls is fixed to $l_i = 1$ mm.

with the procedure shown in [3], with the desired specifications of the filter, leading to

$$M = \begin{bmatrix} 0 & 0.9017 & 0 & 0 & 0 & 0 \\ 0.9017 & 0 & 0.7411 & 0 & 0.2483 & 0 \\ 0 & 0.7411 & 0 & -0.7576 & 0 & 0 \\ 0 & 0 & -0.7576 & 0 & 0.7411 & 0 \\ 0 & 0.2483 & 0 & 0.7411 & 0 & 0.9017 \\ 0 & 0 & 0 & 0 & 0.9017 & 0 \end{bmatrix}. \tag{6}$$

Note that this matrix has all the diagonal elements equal to zero. This means that the topology is synchronously tuned, and all resonators are tuned at the center frequency of the passband. As already mentioned, this is the case when the frequency response to be synthesized is symmetrical with respect to the center frequency. Therefore, in this case all constant susceptances of the equivalent circuit will be equal to zero ($M_{mm} = B_m = 0$). It is also interesting to remark that one of the couplings of the matrix has a negative sign. For the solution shown in (6) this is the coupling (M_{23}). As already mentioned, the folding of the structure along the E-plane allows enough flexibility to adjust the sign of the couplings along the vertical path

(M_{14} and M_{23}). Assuming that the signs of the couplings along the main path are positive, the window (a_4) placed at the center of the cavity as shown in Fig. 4, will produce a coupling (M_{14}) also positive. In order to reverse the sign of the (M_{23}) coupling, as required by the coupling matrix, the window (a_3) needs to be placed at one side of the cavity, as also shown in Fig. 4.

The next step in the design procedure is to calculate the scaled coupling matrix (M'), using as resonators the resonant mode (TE_{101}) in the corresponding rectangular waveguide cavities. We should emphasize that, since all resonators employed in the physical implementation are the same, all the resonators in the equivalent circuit will be identical, and the subindex (m) can be dropped from the notation ($C_{r_m} = C_r$, $L_{r_m} = L_r$). Using the propagation constant (β) of the mode (TE_{10}) in our rectangular waveguide, at the center frequency and at the lower cut-off frequency of the passband [β_0 and β_1, see (3)], equation (1) can be used to compute the lumped elements resonators, obtaining $C_r = 0.086$ pF and $L_r = 2.42$ nH. The use of (4) permits to calculate the scaling factor in the lowpass domain, obtaining ($C_m = C = 163.05$ nF). Finally, for the source and load terminations we should use the information of the real ports that excite the physical structure. As shown in the 3D view of Fig. 3(b) (red areas), the excitation is formed with the TE_{10} mode propagating in the standard WR-75 waveguides (waveguide ports). Using the characteristic impedance of this mode, evaluated again at the center frequency of the passband, we obtain: $Z_S = 1/Y_S = 1/Y_L = 539.116\,\Omega$. With these values, the scaled coupling matrix (M') can be calculated using (5a)-(5c), obtaining

$$M' = 10^{-3} \cdot \begin{bmatrix} 0 & 0.4959 & 0 & 0 & 0 & 0 \\ 0.4959 & 0 & 0.1208 & 0 & 0.0405 & 0 \\ 0 & 0.1208 & 0 & -0.1235 & 0 & 0 \\ 0 & 0 & -0.1235 & 0 & 0.1208 & 0 \\ 0 & 0.0405 & 0 & 0.1208 & 0 & 0.4959 \\ 0 & 0 & 0 & 0 & 0.4959 & 0 \end{bmatrix}. \tag{7}$$

Once the scaled coupling matrix is known, the equivalent circuit of the whole bandpass filter is directly obtained with the calculated values, as shown in Fig. 5. In the step-by-step design technique, this equivalent circuit will be divided in several sub-circuits. The process starts by considering just the first admittance inverter (M'_{S1}), as shown in Fig. 6, representing the input coupling of the structure. The response of this circuit is very simple, as it contains just one constant admittance inverter, as shown with red crosses

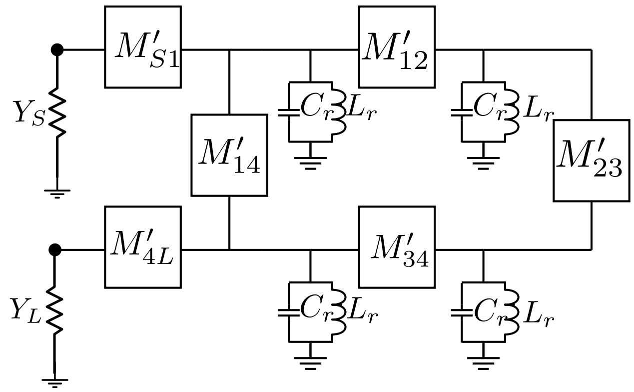

Figure 5: Equivalent circuit of the filter obtained from the scaled coupling matrix (7).

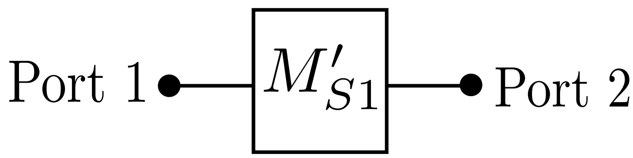

Figure 6: Equivalent circuit of the first segment of the filter. The response of this circuit is used to adjust the input iris of the filter (a_1) in the fist step of the technique.

in Fig. 7. This response is used to optimize the input iris of the physical structure, composed of the inductive window (a_1) shown in Fig. 4. The part of the physical structure that corresponds to the first segment of the equivalent circuit is shown in the panel of Fig. 7. We have to clarify that in this structure the waveguide corresponding to the resonator R_1 is simply terminated by a waveguide port (Port 2 shown in the panel of Fig. 7). We remark that the response of this iris is not constant with frequency, due to the inherent dispersion of inductive irises. However, the iris width (a_1) is adjusted until the right transmission level is retrieved at the center frequency of the passband (f_0), as shown in the plot. Here, full-wave simulations are performed using FEST3D software [17] to evaluate the scattering parameters of the different segments of the physical structure. In this first step, only the width of the input iris (a_1) is obtained, as shown in the second column (Step 1) of Table 1.

For the second step of the design process, the admittance inverters (M'_{12}) and (M'_{14}) are added, together with the first resonator (R_1), giving the equivalent circuit shown in Fig. 8. It can be observed that the subcircuit is now

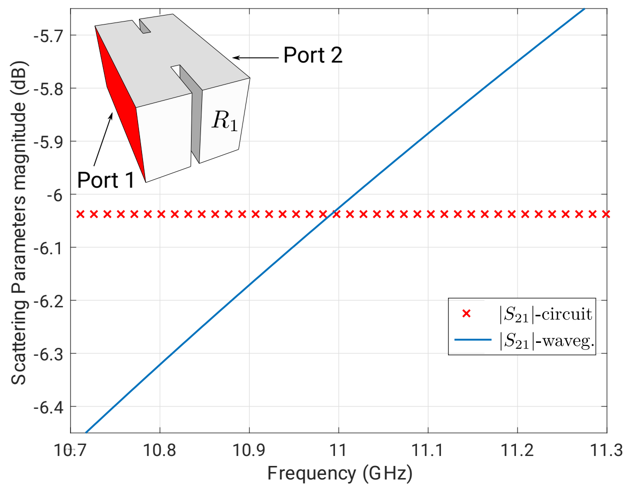

Figure 7: Transmission response ($|S_{21}|$) of the equivalent circuit for the first segment shown in Fig. 6 (red crosses), and similar response of the input inductive iris (a_1) after optimization. The panel shows a 3D sketch of the physical structure corresponding to the first segment.

	Step 1	Step 2	Step 3	Step 4	Final	Error (%)
a_1 (mm)	9.114	9.038	9.038	9.038	9.056	0.20
a_2 (mm)		5.574	5.517	5.517	5.548	0.60
a_3 (mm)			9.407	9.359	9.382	0.24
a_4 (mm)		3.923	3.923	3.923	3.929	0.20
l_1 (mm)		17.228	17.249	17.249	17.226	0.13
l_2 (mm)			18.565	18.553	18.542	0.05

Table 1: Values of all geometrical parameters of the filter obtained after each iteration, and after a global optimization of the whole structure. The relative errors obtained with the design technique proposed are also included in the last column.

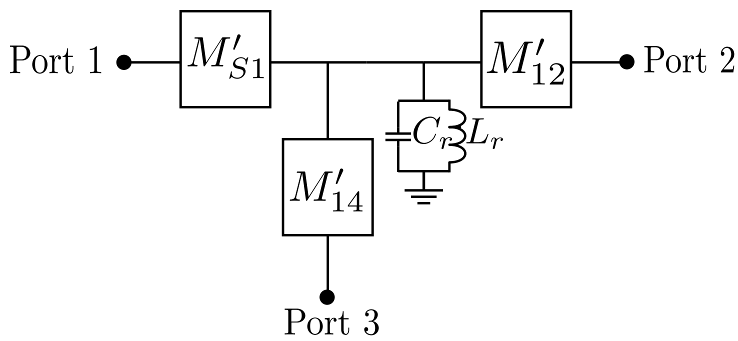

Figure 8: Equivalent circuit of the second segment of the filter. Note that three ports are included to take into account for the two paths of the signal. Port 2 is placed along the main path, while port 3 is placed along the cross-coupling path.

defined with three ports. In this way, it is possible to characterize how the input power must be split between the direct and the cross coupling paths. Therefore, for this second step, two main responses ($|S_{21}|$) and ($|S_{31}|$) will be important to define the optimization operations. Both responses are shown with symbols in Fig. 9, in the relevant bandwidth of the filter. These two responses are simultaneously used to adjust the second segment of the physical structure, which is shown in the panel inside the figure. In the physical structure, the coupling (M'_{12}) is formed with the inductive iris (a_2) shown in Fig. 4. The cross coupling (M'_{14}) is adjusted with the vertical iris (a_4). Finally, the resonant frequency of the first resonator (R_1) is adjusted with the length (l_1). As indicated in the panel of Fig. 9, the waveguide corresponding to resonator R_4 is terminated on the back side with a short circuit, and on the front side with a waveguide port (Port 3). For the simulation, we have selected a length for this waveguide section of ($l_4 = l_1$). Also, the waveguide corresponding to resonator R_2 is terminated with a waveguide port (Port 2).

The main geometrical parameters involved in the optimization operations for this second step of the design process are a_2, a_4 and l_1 (see Fig. 4). The three geometrical parameters are first optimized until the two responses are simultaneously recovered, as shown with solid lines in Fig. 9. Here it should be pointed out that, after a first optimization with these three variables, a small refinement including the input iris (a_1) is usually required. In this way, the interactions and small couplings of all the elements of the structure are rigorously accounted for during the final calculation of the relevant geometrical parameters.

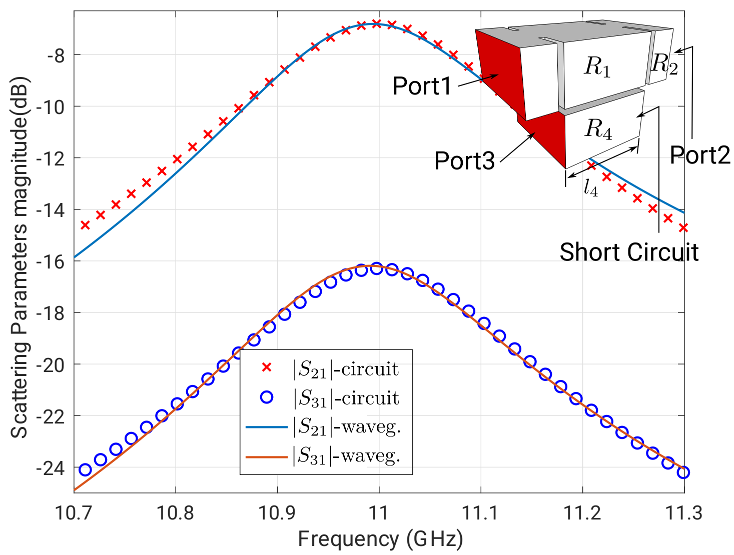

Figure 9: Transmission responses ($|S_{21}|$) and ($|S_{31}|$) of the second segment of the equivalent circuit during the design process (symbols). Solid lines refer to the responses obtained for the corresponding segment of the physical structure (shown in the panel), after optimization.

The geometrical parameters obtained, at this stage of the design process, are collected in the third column of Table 1 (Step 2). In particular, the input iris has been modified from $a_1 = 9.114$ mm in Step 1 to $a_1 = 9.038$ mm in Step 2. This indicates that, although small, the interactions and loading effects of the first resonator and the cross coupling on this iris are important, resulting into a final variation of about 0.8%. The result also illustrates the importance of taking into account for coupling effects and interactions from neighboring elements, during the final adjustment of the different parts of the structure.

In the third step of the design process, we propose to continue the monitorization of the signal into both main and cross coupling paths, but we add a new coupling (M'_{23}) and a new resonator (R_2) into the main path of the equivalent circuit, as shown in Fig. 10. It can be observed in the figure that the equivalent circuit again contains three ports. This allows to monitor at the same time the signal along the main path and along the cross coupling path. Consequently, two transmission functions ($|S_{21}|$ and $|S_{31}|$) will be used simultaneously in the optimization problem, as shown with symbols

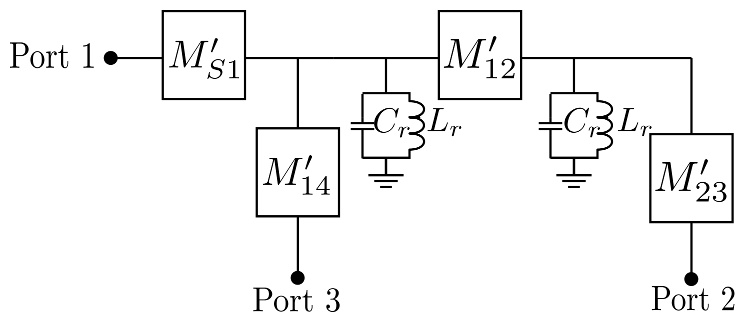

Figure 10: Equivalent circuit of the third segment of the filter. The signal along the main and the cross coupling paths are still monitored by using three ports. However, a new coupling (M'_{23}) and the second resonator is added to the main path.

in Fig. 11.

In the physical structure, the new coupling is adjusted with the iris (a_3), while the new resonator is adjusted with the length (l_2), as shown in Fig. 4. As illustrated in the panel of Fig. 11, the waveguide associated to resonator R_4 is again terminated on the back side with a short circuit and on the front side with a waveguide port (Port 3). The waveguide associated to resonator R_3 is terminated in the same way, having on the front side the waveguide port (Port 2). For the simulations of this sub-structure, we have selected: $l_4 = l_1$ and $l_3 = l_2$ (see Fig. 4).

Following the same strategy as before, the new geometrical parameters (a_3 and l_2) are first optimized to recover simultaneously the responses shown in Fig. 11. After this first optimization process, a refinement is conducted including also neighboring elements (a_2, a_4, l_1). Note that at this stage, the input iris (a_1) does not need to be included in the optimization process. This refinement operation allows to recover with high accuracy the multiport goal functions of the equivalent circuit, as shown with solid lines in Fig. 11.

The geometrical dimensions obtained after this step are included in the fourth column of Table 1 (Step 3). This shows that the important parameters in the optimization are the new iris width (a_3) and resonator length (l_2). In fact, the previous width (a_2) and length (l_1) vary little with respect to the previous step, showing relative variations of 1% and 0.1%, respectively. The iris width (a_4), controlling the cross coupling, also shows a small variation of 0.15% with respect to the value obtained in the previous step. In any case, these variations suggest again the importance of considering nearby elements during the final adjustment of the different parts of the structure.

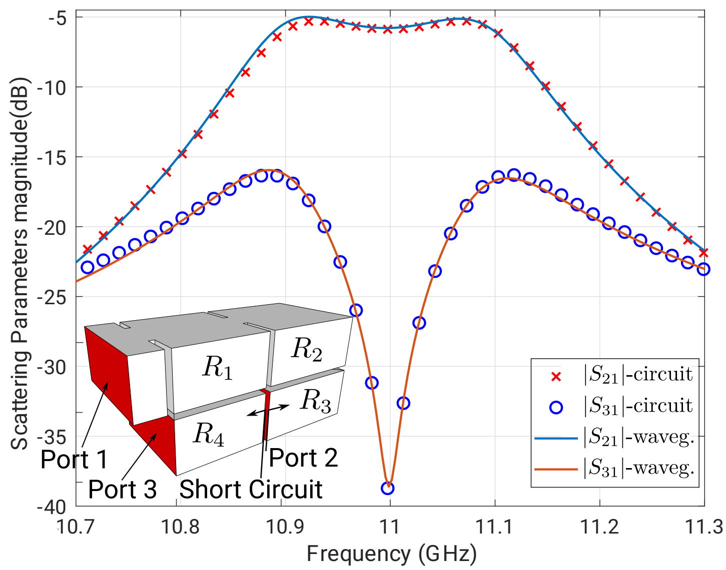

Figure 11: Transmission functions ($|S_{21}|$ and $|S_{31}|$) of the equivalent circuit proposed for the third step of the design process (symbols). Solid lines show the responses of the physical structure corresponding to the third segment (shown also in the panel), after optimization.

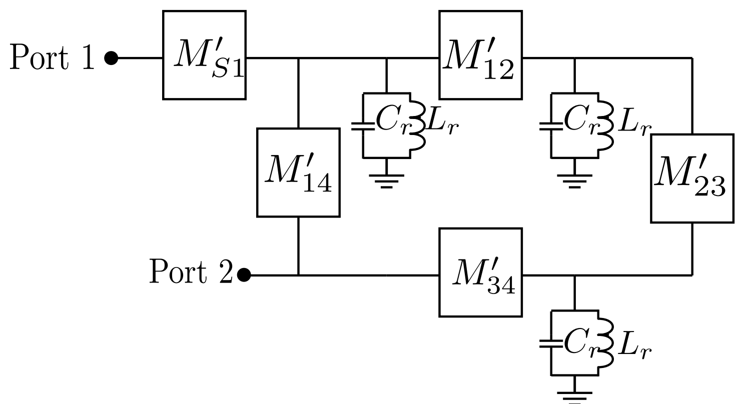

Figure 12: Equivalent circuit of the fourth segment of the filter. In this last step of the design process only two ports are used.

At this point, after three iterations, all the geometrical parameters corresponding to the first half of the filter have been calculated. However, it is convenient to perform an additional step of the design procedure, in order to take into account for nearby elements in the last components of the filter. In this last step we will add the next resonator (R_3) and coupling (M'_{34}) along the main path, obtaining the equivalent circuit shown in Fig. 12. It can be observed that in this last step only two ports are considered in the equivalent circuit. In fact, the main and the cross coupling paths are joined together in the output port of the subcircuit (Port 2). Therefore, this time only one objective function is used in the optimization problem ($|S_{21}|$). The physical segment corresponding to this subcircuit is shown in the panel of Fig. 13. It can be observed that the waveguides corresponding to resonators (R_3) and (R_4) are coupled by an additional inductive window, while the waveguide corresponding to (R_4) is used to place the output Port 2 of the segment.

In the optimization problem, we first adjust the last coupling window and the length of the third resonator [l_3 in Fig. 4(b)]. This first optimization operation leads to a coupling window of 5.504 mm. However, due to the symmetry of the structure, this value will be discarded when computing the final filter geometry. The important task now is to refine the response shown in Fig. 13 with symbols (circuit response) by including also the previous coupling window (a_3) and the previous resonator length (l_2). By including these two previous elements, the response of the subcircuit is retrieved with great accuracy, as can be observed in Fig. 13 (solid line). It is interesting to

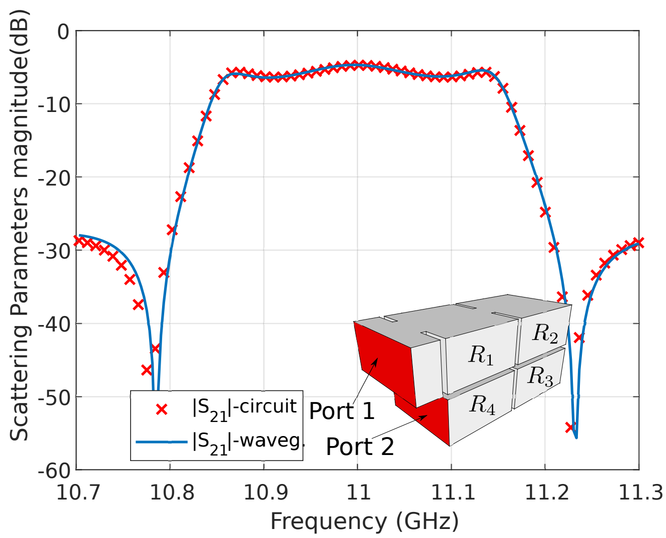

Figure 13: Transmission function ($|S_{21}|$) of the equivalent circuit proposed for the fourth step of the design process (symbols). Solid line shows the response of the physical structure corresponding to the fourth segment (shown also in the panel), after optimization.

note that to obtain this response the window along the cross coupling path (a_4) was not modified. The accuracy obtained in the coupling (a_3) and in the length of the second resonator (l_2) is increased, since the interactions of additional nearby elements are included during the last optimization process. The geometrical parameters obtained after this refinement operation are included in the fifth column of Table 1 (Step 4). The table shows that the coupling width (a_3) and the length (l_2) have slightly varied, with relative errors of (0.51%) and (0.06%) with respect to the previous step.

The geometrical parameters shown in Table 1 for Step 4 are considered to be the initial design, directly obtained from the proposed method. Fig. 14 shows the target response of the coupling matrix and the response of the physical structure with these initial dimensions. In general, it can be observed good agreement between both responses. Since the initial design obtained with the proposed technique is very close to the target specifications, a global optimization process using gradient techniques can be used to improve the solution. In Table 1 we include the final dimensions obtained after the global optimization of the structure, and the response is shown, for comparison, in Fig. 14. It can be observed good agreement with respect to the target response given by the coupling matrix. In particular the target return loss

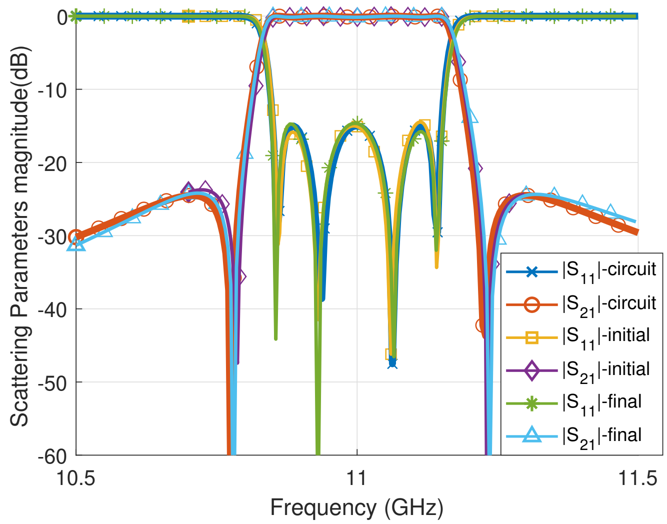

Figure 14: Comparison between the target response of the filter provided by the coupling matrix, and the response of the physical structure with the dimensions directly obtained from the proposed design technique. The response of the physical structure after applying a global optimization process is also shown.

level inside the passband of $RL = 15$ dB has been obtained. In the last column of Table 1, we further show the relative errors obtained in all the geometrical parameters of the filter. Relative errors are defined between the values obtained directly after the design process, and those obtained after the global optimization. Results demonstrate high accuracy of the proposed design strategy, as relative errors as low as 0.6 % are systematically obtained.

4. Altenative design

The design technique illustrated in the previous section with a quartet example exhibiting two transmission zeros in the real frequency axis, can also be used for the design of a similar filter structure, but with complex transmission zeros placed at the center of the passband. These complex transmission zeros are used in filtering functions to achieve flat group delay responses. Therefore, it is interesting to demonstrate that the design technique proposed in this paper is also valid for the design of filters exhibiting this type of alternative transfer functions.

The in-band characteristics of the filter are the same as indicated for the

	Initial	Final	Error (%)
a_1 (mm)	9.154	9.189	0.38
a_2 (mm)	5.8089	5.819	0.17
a_3 (mm)	5.150	5.129	0.41
a_4 (mm)	4.312	4.358	1.06
l_1 (mm)	17.173	17.147	0.15
l_2 (mm)	19.306	19.308	0.01

Table 2: Dimensions of the filter in quartet topology with two complex transmission zeros. Dimensions obtained directly after the application of the design technique can be compared to those obtained after a global optimization. Last column shows the relative errors obtained between the initial and final optimized dimensions. The structure follows the same sketch of Fig. 4, but the iris (a_3) is placed at the center of the cavity.

previous design (f_0 = 11 GHz, BW = 300 MHz, RL = 15 dB). However, complex transmission zeros are placed at the center of the passband to reduce the group delay variation. After adjusting the positions of the transmission zeros in the complex plane, the normalized coupling matrix results to be

$$M = \begin{bmatrix} 0 & 0.9379 & 0 & 0 & 0 & 0 \\ 0.9379 & 0 & 0.8177 & 0 & 0.3120 & 0 \\ 0 & 0.8179 & 0 & 0.4899 & 0 & 0 \\ 0 & 0 & 0.4899 & 0 & 0.8177 & 0 \\ 0 & 0.3120 & 0 & 0.8177 & 0 & 0.9379 \\ 0 & 0 & 0 & 0 & 0.9379 & 0 \end{bmatrix}. \tag{8}$$

The design of this filter essentially follows the same steps as described in the previous section. The only relevant change is in the sign of the (M_{23}) coupling, which is now positive as shown in (8). This modification can be easily introduced in the physical structure, due to the fact that it is folded in the E-plane. The sign change is simply implemented by placing the vertical iris (a_3 shown in Fig. 4) at the center of the second cavity [R_2 indicated in Fig. 3(b) and Fig. 4(b)].

After following the same steps detailed in the previous section, the dimensions obtained for the filter are collected in the second column of Table 2 (Initial). The response obtained for this structure, as compared to the target response of the coupling matrix (8) is presented in Fig. 15. It can be observed that the response obtained directly from the proposed design technique agrees very well with respect to the reference response. Due to the

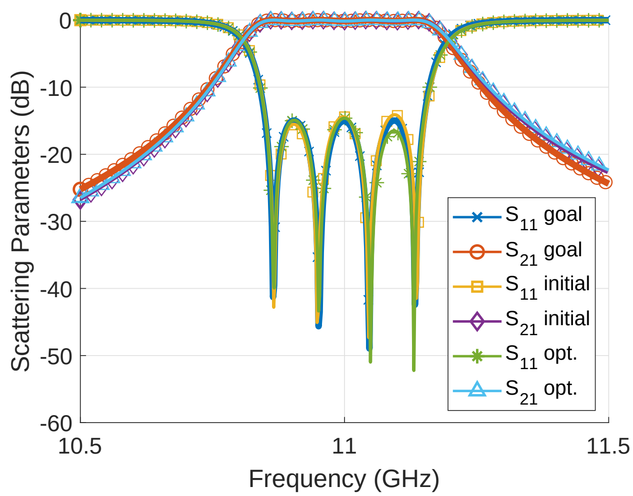

Figure 15: Comparison between the response obtained for the filter in quartet topology with two complex transmission zeros, and the reference response given by the coupling matrix (8). Results before and after performing a global optimization on the structure are shown.

high quality of the initial design, a global optimization using gradient techniques converges easily, and allows to improve the response, as also shown in Fig. 15. In Table 2 we also collect for completeness the dimensions obtained after the final global optimization (Final). In the last column, we also give the relative errors between the solution directly obtained from the proposed design technique and the one obtained after the global optimization. In this case, all relative errors are below 1.06%.

To show the effectiveness of this solution in the equalization of the group delay, we present this electrical characteristic in Fig. 16. The figure shows the group delay of the filter, and compares it to the reference solution given by the coupling matrix (8). The group delays are given for the filter directly obtained from the design technique, and for the filter after applying the global optimization operation. For reference, the group delay of the filter in quartet topology with the transmission zeros in the real frequency axis is also included. Results clearly show that a significant reduction in group delay variation can be achieved by placing the transmission zeros in the complex plane, at appropriate locations. Results also show very good agreement of the group delay of the designed filter with respect to the reference solution provided by the coupling matrix. In any case, this second example also demonstrates the usefulness of the proposed strategy, in the design of this

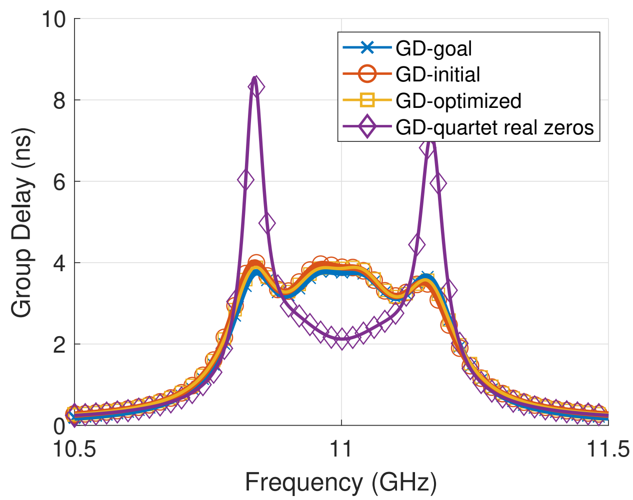

Figure 16: Group delay obtained for the filter in quartet topology with complex transmission zeros, as compared to the group delay given by the coupling matrix (8) (crosses). The group delay of the filter obtained directly after the design process (circles) and after a global optimization (squares) are shown. For comparison, the group delay of the filter in quartet topology with transmission zeros in the real frequency axis (diamonds) is also included.

type of folded canonical topologies implementing complex transmission zeros.

5. Conclusions

In this work, a strategy to design filters in folded canonical topologies is presented. The technique is based on scaling the normalized coupling matrix to find useful partial responses of the filter equivalent circuit. This work proposes for the first time the optimization of the different segments of the structure using multiport networks. This allows to consider several goal functions in the equivalent circuit, which are simultaneously used in the optimization problem of the different segments of the physical structure. In this way, the signal can be monitored along the main path and along the cross coupling paths, usually present in this type of topologies. The proposed technique has been successfully applied to the design of two filters in quartet topology, one with two transmission zeros in the real frequency axis, and the other with complex transmission zeros. The results confirm that the proposed technique leads to initial designs that are very close to the desired target specifications. Similar strategy, as introduced in this paper, can be applied to the design of other filters in folded canonical topologies of higher orders or containing additional cross couplings.

6. Acknowledgment

This work has been developed with funding from Thales Alenia Space (Tres Cantos, Madrid, Spain) in the project *"Diseño e implementación de nuevas estructuras de filtros de microondas usando la técnica de fabricación aditiva"*, and from *Ministerio de Economía y Competitividad* with the project *"Análisis y Diseño de Nuevos Componentes de Microondas y Milimétricas para Comunicaciones por Satélite (MILISAT)"* with Ref. TEC2016-75934-C4-4-R.

Bibliography

References

[1] G. Matthaei, L. Young, E. Yones, Microwave Filters, Impedance Matching Networks, and Coupling Structures, Artech House, Boston, Massachusetts, USA, 1980 (1980).

[2] J. Hong, M. Lancaster, Microstrip filters for RF/Microwave Applications, John Wiley & Sons, USA, 2001 (2001).

[3] R. J. Cameron, C. M. Kudsia, R. R. Mansour, Microwave Filters for Communication Systems, Wiley, 2007, pp. 379–386, ISBN: 978-0-471-45022-1 (2007).

[4] D. Goldberg, Genetic Algorithm in Search, Optimization and Machine Learning, Addison-Wesley, 1989, Ch. 3, pp. 60–88 (1989).

[5] M.-I. Lai, S.-K. Jeng, Compact microscript dual-band bandpass filters design using genetic-algorithm techniques, IEEE Transactions on Microwave Theory and Techniques 54 (1) (2006) 160–168 (January 2006).

[6] W. Wang, Y. Lu, J. S. Fu, Y. Z. Xiong, Particle swarm optimization and finite-element based approach for microwave filter design, IEEE Transactions on Magnetics 41 (5) (2005) 1800–1803 (May 2005). doi:10.1109/TMAG.2005.846467.

[7] S. K. Goudos, J. N. Sahalos, Pareto optimal microwave filter design using multiobjective differential evolution, IEEE Transactions on Antennas and Propagation 58 (1) (2010) 132–144 (Jan 2010). doi:10.1109/TAP.2009.2032100.

[8] J. W. Bandler, Q. S. Cheng, S. A. Dakroury, A. S. Mohamed, M. H. Bakr, K. Madsen, J. Sondergaard, Space mapping: The state of the art, IEEE Transactions on Microwave Theory and Techniques 52 (1) (2004) 337–361 (January 2004).

[9] M. Sans, J. Selga, A. Rodriguez, J. Bonache, V. E. Boria, F. Martin, Design of planar wideband bandpass filters from specifications using a two-step aggressive space mapping (ASM) optimization algorithm, IEEE Transactions on Microwave Theory and Techniques 62 (12) (2014) 3341–3350 (December 2014).

[10] J. Hinojosa, F. D. Quesada-Pereira, M. Martinez-Mendoza, A. Alvarez-Melcon, Optimization-oriented design of RF/microwave circuits using inverse-linear-input neuro-fuzzy-output space mapping with two different dimensionality simulators, IEEE Transactions on Circuits and Systems I: Regular Papers 58 (1) (2011) 176–185 (Jan 2011). doi:10.1109/TCSI.2010.2055314.

[11] J. Hinojosa, F. D. Quesada-Pereira, M. Bozzi, A. Alvarez-Melcon, Efficient optimization-oriented design methodology of high-order 3-D filters using 2-D and 3-D electromagnetic simulators, International Journal of Circuit Theory and Applications 43 (10) (2015) 1431–1445 (2015). doi:10.1002/cta.2008.
URL `http://dx.doi.org/10.1002/cta.2008`

[12] J. Tucker, P. Bhartia, P. Pramanick, A new waveguide filter design and optimization approach using shadow specifications, AEU - International Journal of Electronics and Communications 56 (6) (2002) 380 – 388 (2002). doi:https://doi.org/10.1078/1434-8411-54100126.

[13] S. Cogollos, M. Brumos, V. E. Boria, C. Vicente, J. Gil, B. Gimeno, M. Guglielmi, A systematic design procedure of classical dual-mode circular waveguide filters using an equivalent distributed model, IEEE Transactions on Microwave Theory and Techniques 60 (4) (2012) 1006–1017 (April 2012). doi:10.1109/TMTT.2012.2183381.

[14] M. Guglielmi, A simple CAD procedure for microwave filters and multiplexers, IEEE Transactions on Microwave Theory and Techniques 42 (7) (1994) 1347–1352 (July 1994).

[15] M. Guglielmi, A. Alvarez-Melcon, Novel design procedure for microwave filters, in: EuMC, European Microwave Conference, EuMC, 1993, pp. 212–213 (6-9 September 1993).

[16] D. Martinez-Martinez, A. Pons-Abenza, A. Romera-Perez, J. Hinojosa, F. Quesada-Pereira, A. Alvarez-Melcon, M. Guglielmi, Advanced filter design technique based on equivalent circuits and coupling matrix segmentation, International Journal of Circuit Theory and Applications 46 (5) (2018) 1055–1071 (2018). arXiv:https://onlinelibrary.wiley.com/doi/pdf/10.1002/cta.2480, doi:10.1002/cta.2480.

[17] Dassault Systemes, FEST3D, https://www.3ds.com/products-services/simulia/products/fest3d/.